Efficient Nonlinear Actuator Fault Reconstruction System

Lu, Peng; van Kampen, Erik-Jan; Chu, Qiping

DOI
10.2514/6.2017-1263

Publication date
2017

Document Version
Accepted author manuscript

Published in
AIAA Guidance, Navigation, and Control Conference, 2017

This is an Accepted Manuscript of an article published in: AIAA Guidance, Navigation, and Control Conference January 9-13, Grapevine, TX. ISBN: 978-1-62410-450-3
Available online: https://arc.aiaa.org/doi/10.2514/6.2017-1263

Efficient Nonlinear Actuator Fault Reconstruction System

P. Lu*, E. van Kampen†, and Q.P. Chu‡
Delft University of Technology, Delft, 2600 GB, The Netherlands

This paper presents an actuator fault reconstruction system for civil aircraft. The fault reconstruction uses the 'local' actuator model and the sensor measurements. Five different actuator benchmark faults are considered: liquid and solid Oscillatory Failure Case (OFC), liquid and solid jamming, and runaway. The OFC reconstruction is regarded as an input fault reconstruction and is achieved by designing an Iterated Optimal Two-Stage Extended Kalman Filter (IOTSEKF) whereas jamming and runaway faults are considered as output faults and are reconstructed by designing a Robust Three-Step Extended Kalman Filter (RTS-EKF). In all the scenarios, both the state and faults are estimated in an unbiased sense. The accurate estimated state is fed back to the control system of the actuator which is designed using the Nonlinear Dynamic Inversion (NDI) approach. The complete actuator fault reconstruction system is presented. Simulation results demonstrate the effectiveness of the proposed system, which shows that the presented system can be applied in practice.

Nomenclature

F	=	the distribution matrix of the output fault
N	=	gain matrix of the output fault
Q_k, R_k	=	covariance matrices of the process noise and measurement noise
q	=	rod position
g	=	distribution matrix of the input
$\dot{q}$	=	velocity of the piston
$\frac{\Delta P}{P_s}$	=	normalized pressure difference
u	=	the input of the actuator
f	=	nonlinear function of the system model
h	=	nonlinear function of the measurement model
f^i	=	input faults, including liquid and solid OFC
f^o	=	output faults, including liquid and solid jamming and runaway
$\mathbf{x}$, u, y	=	state vector, input and output
$\hat{x}$	=	estimation of the states
$\hat{f}^i$, $\hat{f}^o$	=	estimation of input faults and output faults
P	=	error covariance matrix of the estimation
γ	=	innovation of the filter
n, m, p	=	the dimension of the state, output and output faults
y	=	output of the actuator

*Ph.D. Student, Control and Simulation Division, Faculty of Aerospace Engineering, P.O.Box 5058; P.Lu-1@tudelft.nl, Student Member AIAA.
†Assistant Professor, Control and Simulation Division, Faculty of Aerospace Engineering, P.O.Box 5058; E.vanKampen@tudelft.nl, Member AIAA.
‡Associate Professor, Control and Simulation Division, Faculty of Aerospace Engineering, P.O.Box 5058; q.p.chu@tudelft.nl, Member AIAA.

I. Introduction

In the last few decades, Fault Detection and Isolation (FDI) has played an important role in increasing the safety of the aircraft. Model-based approach is a good candidate to achieve FDI. Many approaches are proposed which make use of the model information.[1,2,3] Recent work related to the FDI, the Advanced Fault Diagnosis for Sustainable Flight Guidance and Control (ADDSAFE), focuses on the sensor and actuator faults of civil aircraft.[4] Indeed, both sensor and actuator faults can result into flight accidents. During the last few decades, many FDI approaches have been proposed for aircraft.[5,6] For applications in aerospace engineering such as civil aircraft, low computational load is still a limitation for the design of most model-based FDI approaches. On the other hand, most real-life models are not exact, which leads into model uncertainties. Consequently, model-based approaches face another challenge - robustness to model uncertainties. As such, low computationally intensive approaches with better robustness to model uncertainties are preferred. As for sensor FDI, one feasible approach is to use the kinematic model[7,8] which does not use the aerodynamic model of the aircraft and has less model uncertainties. Many approaches based on this model show good potential.[8,9,10,11,12] In terms of actuator FDI, one suitable solution is to use the "local" model of the actuator instead of using the aerodynamic model of the aircraft. Different approaches are proposed based on the actuator model.[13,14,15]

There are different actuator faults which have different influences on the aircraft. Oscillatory Failure Case (OFC) is a failure case which may be generated by the electrical flight control system. If the oscillatory failures are coupled with the aeroelastic behaviour of the aircraft, they may lead to unacceptable structural loads.[13] Therefore, the capability to detect these faults is very important.

This paper deals with the actuator fault reconstruction problem. In order to save the computational load, this paper does not use the aerodynamic model of the aircraft which contains the calculation of the aerodynamic forces and moments. Since exact aerodynamic forces and moments are difficult to obtain, using the aerodynamic model may lead to model uncertainties. Instead, it uses the local actuator model as the model for the fault reconstruction. In this situation, it saves the computational load and reduces the influence of model uncertainties.

The model used in the present paper is a generic actuator model which can represent the dynamics of the civil aircraft actuator. First the modeling of the actuator is given. Then, a Nonlinear Dynamic Inversion (NDI) controller is designed for the actuator model which controls the rod position of the actuator.

The main contribution of this paper is that it proposes a complete actuator fault reconstruction system which deals with five different actuator fault scenarios: liquid OFC, solid OFC, liquid jamming, solid jamming and runaway. The five different fault scenarios are considered as two different fault types. The liquid and solid OFC are considered as input faults of the actuator whereas the liquid and solid jamming and runaway are treated as output faults of the actuator. Therefore, two different fault reconstruction schemes are required which are as follows.

For input fault reconstruction, an Iterated Optimal Two-Stage Extended Kalman Filter (IOTSEKF) is proposed which can estimate both the state and fault in an unbiased sense. Therefore, the liquid and solid fault reconstruction is obtained.

For output fault reconstruction, a Robust Three-Step Extended Kalman Filter (RTS-EKF) is introduced which can estimate the state and the output fault in an unbiased sense. Hence, the liquid and solid jamming and runaway fault can be reconstructed.

The estimated state is used by the controller to generate control laws. All the five different fault scenarios are considered in the paper. The simulation results demonstrate the performance of the proposed fault reconstruction system. All the faults are estimated in an unbiased sense together with the unbiased estimation of the states. This indicates that the proposed fault reconstruction system has a potential to be applied in real application to enhance the safety of the civil aircraft.

The structure of the paper is as follows: Section II presents the generic actuator model and the fault scenarios which are considered in the paper. The complete actuator fault reconstruction system is proposed in section III. The controller design is also introduced in this section. The specific fault reconstruction schemes are introduced in sections IV and V respectively. Section IV presents the reconstruction scheme for the input faults which makes use of the IOTSEKF. Both the liquid and solid OFC is reconstructed using this scheme. Section V presents the reconstruction strategy for the output faults which makes use of the RTS-EKF. The liquid and solid jamming and runaway are reconstructed using this scheme. The states are also estimated by the fault reconstruction system and used by the controller. All the fault scenarios are simulated. Finally, the conclusions are made in section VI.

II. Modeling of the hydraulic actuator and faults

This section presents the generic actuator model and the fault scenarios. In section A, the actuator model including input and output faults are presented. In section B, five actuator fault scenarios are presented which will be dealt with in this paper.

The reason why the local actuator model instead of the aerodynamic model is used for the actuator fault reconstruction is that using the local model can reduce the computational load and does not require the calculation of the aerodynamic forces and moments.

A. Modeling of hydraulic actuator

A generic hydraulic actuator model including input and output faults can be modeled as follows:[16,17]

$$\dot{\mathbf{x}}(t) = f(\mathbf{x}(t), u(t), f^i(t)) + w(t) \tag{1}$$

$$y(t) = h(\mathbf{x}(t), f^o(t)) \tag{2}$$

$$y_m(t) = y(t) + v(t), t = t_i, i = 1, 2, ... \tag{3}$$

with $\mathbf{x} \in \mathbb{R}^n$ the state vector, $y \in \mathbb{R}^m$ the output, $y_m \in \mathbb{R}^m$ is the measured output. w and v are the process and measurement noise with covariances $E\{w(t_k)w(t_l)^T\} = Q_k\delta_{kl}$, $E\{v(t_k)v(t_l)^T\} = R_k\delta_{kl}$ and $E\{w(t_k)v(t_l)^T\} = 0$ where δ_{kl} is the Kronecker function, k and l are the time steps. f and h are nonlinear functions, u the input. f^i and $f^o \in \mathbb{R}^p$ are the input and output faults. The nonlinear functions f and h can be given by

$$f(\mathbf{x}, u, f^i) = \begin{cases} x_2 \\ (A_p P_s x_3 - B x_2 + F_d)/M \\ \frac{2A_p E V_m}{P_s(V_m^2 - A_p^2 x_1^2)}\left(\frac{\phi_n}{A_p}\sqrt{1 - \text{sign}(u)x_3}(u + f^i) - L x_3 - x_2\right) \end{cases} \tag{4}$$

$$h(\mathbf{x}, f^o) = x_1 + f^o \tag{5}$$

with the state vector defined as

$$\mathbf{x} = [x_1,\ x_2,\ x_3]^T = [q,\ \dot{q},\ \frac{\Delta P}{P_s}] \tag{6}$$

where x_1 represents the position of the actuator rod, x_2 the velocity and x_3 the pressure difference between the actuator chambers. Furthermore, $A_p = 0.0025$ m^2 is the piston area, $B = 52.3$ N·s/m is a damping coefficient, F_d denotes the external forces, $P_s = 1.4 \times 10^7$ N/m^2 the reservoir oil pressure, $\phi_n = 0.0025$ m^3/s the maximum valve flow, $V_m = 0.001973$ m^3 the mean actuator chamber volume, $E = 10^9$ N/m^2 the oil bulk modulus, $M = 2000$ kg the mass of moving system and $L = 0.023$ m/s the normalized leakage parameter.

B. Actuator fault scenarios

In this paper, we consider five benchmark fault scenarios given in Table 1.

Table 1: Actuator fault scenarios

Scenario	Fault	Occurrence time
1	liquid OFC	$t = 12$ s
2	solid OFC	$t = 12$ s
3	liquid jamming	$t = 12$ s
4	solid jamming	$t = 12$ s
5	runaway	$t = 12$ s

As can be seen from Table 1, there are three types of faults: OFCs, jamming and runaway. The OFC includes liquid and solid OFC and the jamming also includes liquid and solid jamming. The definition of the faults and the negative effect of these faults will be detailed in the following sections.

III. Actuator fault reconstruction system

This section introduces the complete actuator fault reconstruction system. First, Section A designs an NDI controller for the actuator servo loop. Then, section B presents the complete actuator fault reconstruction system with the explanations of each block.

A. Design of the actuator controller

Here we design a controller for the nominal case. Therefore,by assuming $f^i = 0$ and $f^o = 0$, we can rewrite the system model Eqs. (1) and (2) into the following affine-in-control form:

$$\dot{\mathbf{x}} = f(\mathbf{x}) + g(\mathbf{x})u \tag{7}$$

$$y = h(\mathbf{x}) \tag{8}$$

with

$$f(\mathbf{x}) = \begin{bmatrix} x_2 \\ (A_p P_s x_3 - B x_2 + F_d)/M \\ \frac{2A_p E V_m}{P_s(V_m^2 - A_p^2 x_1^2)}\big(- L x_3 - x_2\big) \end{bmatrix} \tag{9}$$

$$h(\mathbf{x}) = x_1 \tag{10}$$

$$g(\mathbf{x}) = \begin{bmatrix} 0 \\ 0 \\ \frac{2EV_m\phi_n}{P_s(V_m^2 - A_p^2 x_1^2)}\sqrt{1 - \text{sign}(u)x_3} \end{bmatrix} \tag{11}$$

Now calculate the rth order derivative of the output and denote it in the form

$$\frac{d^r y}{dt^r} = L_f^r h(x) + L_g L_f^{r-1} h(x) u \tag{12}$$

where $L_f^r h(x)$ and $L_g L_f^{r-1} h(x)$ are the Lie derivatives. r is the relative degree of the system, in this paper, $r = 2$. The control input can be given by the following:

$$u = (L_g L_f^{r-1})^{-1}(\nu - L_f^r h(x)) \tag{13}$$

where ν is the linear controller which can be designed, using classical control method such as PID control, based on the error between q_{ref} and q. q_{ref} is the rod position reference for the NDI controller. By now, the controller of the actuator is designed.

B. The actuator fault reconstruction system

The complete actuator fault reconstruction system is given in Fig. 1. As can be seen from the figure, the faults can affect the dynamics of the actuator and the sensor. Three blocks needs to be designed which are as follows:

1. The reference model
   This block is used to generate a reference for the servo controller, denoted by q_{ref} given the command q_{com}. Normally, it can be designed using a third-order low-pass filter.

2. NDI controller
   The controller controls the rod position of the actuator given the reference q_{ref}. The reason why a nonlinear controller is designed is that the actuator system described by Eqs. (1) and (2) is quite nonlinear. A nonlinear controller can reduce the influence of linearizaton errors. The design of the controller has been introduced above.

3. Fault reconstruction
   This block uses the measured rod position y_m to estimate the states of the actuator and also the faults in the actuator loop. The NDI controller uses the estimated states $\hat{x}$ by the fault reconstruction instead of the measured rod position y_m.

Due to the properties of the faults, two different fault reconstruction subsystems have to be designed: input fault reconstruction and output fault reconstruction. These are introduced in the following two sections.

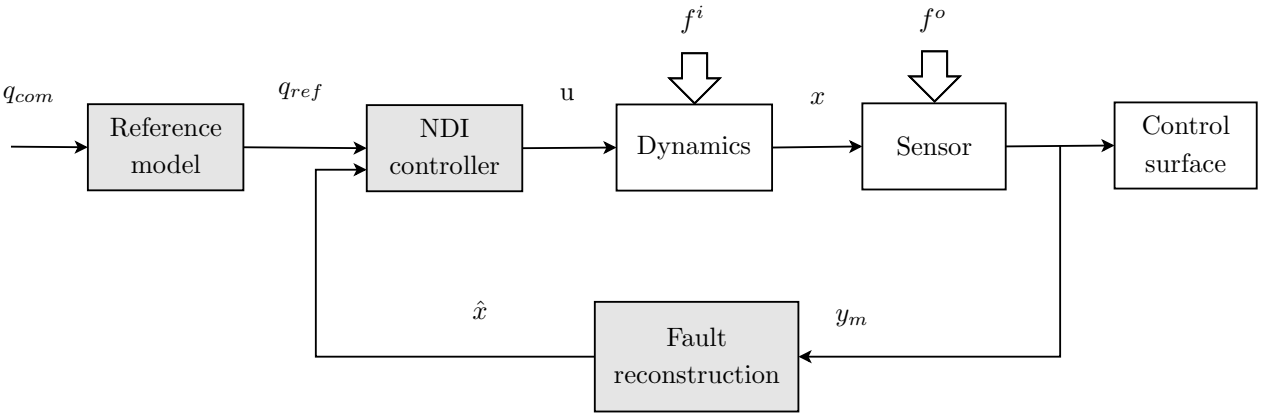

Figure 1: Block diagram of the actuator fault reconstruction system

IV. Actuator OFC Fault Reconstruction

This section designs the fault reconstruction in the presence of OFC. First, some introduction of the OFC is given in Section A. Section B presents the IOTSEKF which will be used to cope with the OFC. Section C presents the results of the fault-free case where no faults are injected. Section D presents the results of the liquid OFC reconstruction using the IOTSEKF while section E demonstrates the results of the solid OFC reconstruction.

A. OFC

An OFC is a type of electrical flight control system failure which results into an control surface oscillations. In this paper, only the OFC located in the servo-loop control of the moving surfaces is considered, which is the case in the ADDSAFE benchmark problem.[13] This OFC is mainly caused by the electronic components in fault mode generating spurious sinusoidal signals.[13] This oscillatory signal propagates through the servo-loop control and results into control surface oscillations.

Two types of OFCs are considered: liquid and solid OFC which is fault scenario 1 and 2 respectively. The liquid OFC adds to the normal signal whereas the solid OFC replaces the normal signal.[13]

According to the above definition, the OFC in this paper can be considered as an input fault of the actuator, which can be represented by f^i. The objective of the fault reconstruction system is to estimate both the state and the fault. Therefore, the IOTSEKF[12] can be used to achieve the fault reconstruction. The introduction of the IOTSEKF is introduced in the following section.

B. Iterated Optimal Two-Stage Kalman Filter

This section first presents the equations of the IOTSEKF for the estimation of f^i (OFC). The IOTSEKF can estimate the state and fault of the system in an optimal minimum variance error sense.[18] It is composed of a modified bias-free filter and a bias filter.[18,12] The IOTSEKF is able to cope with nonlinear systems.

According to Hsieh et al.,[18] the input fault f_k^i is modeled as follows:

$$f_k^i = f_{k-1}^i + w_{k-1}^{f^i} \tag{14}$$

where $w_{k-1}^{f^i}$ is a zero-mean white noise sequence with covariances: $E\{w_k^{f^i}(w_l^{f^i})^T\} = Q_k^{f^i}\delta_{kl}$ and $E\{w_k(w_l^{f^i})^T\} = Q_k^{xf^i}\delta_{kl}$.

The state estimate and its covariance matrix using the IOTSEKF are given as follows:

$$\hat{x}_{k|k} = \bar{x}_{k|k} + V_k\hat{f}_{k|k}^i \tag{15}$$

$$P_{k|k}^x = P_{k|k}^{\bar{x}} + V_k P_{k|k}^{f^i} V_k^T \tag{16}$$

The bias-free filter of the IOTSEKF is as follows:[18,12]

$$\eta_1 = \bar{x}_{k|k-1} = \bar{x}_{k-1|k-1} + \int_{t_{k-1}}^{t_k} f(\bar{x}, u(t), 0)dt + \bar{u}_{k-1} \tag{17}$$

$$P^{\bar{x}}_{k|k-1} = \Phi_{k-1} P^{\bar{x}}_{k-1|k-1} \Phi^T_{k-1} + \bar{Q}_{k-1} \tag{18}$$

where Φ_{k-1} is calculated as follows:

$$\Phi_{k-1} = e^{A_{k-1}\Delta t} = \sum_n^{\infty} \frac{A^n_{k-1}(\Delta t)^n}{n!}, A_{k-1} = \left.\frac{\partial f(x(t), u(t), f^i(t))}{\partial x}\right|_{x=\hat{x}_{k-1|k-1}} \tag{19}$$

$$\Gamma_{k-1} = \int_{t_{k-1}}^{t_k} \Phi_{k-1} G(\bar{x}_{k-1|k-1})d\tau \tag{20}$$

The iteration part of the bias-free filter is as follows:

1. Kalman gain calculation:

$$H_k = \left.\frac{\partial h(x(t), f^o(t))}{\partial x}\right|_{x=\eta_1} \tag{21}$$

$$K^{\bar{x}}_k = P^{\bar{x}}_{k|k-1} H^T_k (H_k P^{\bar{x}}_{k|k-1} H^T_k + R_k)^{-1} \tag{22}$$

2. Measurement update

$$\eta_2 = \bar{x}_{k|k-1} + K^{\bar{x}}_k \big(y_k - h(\eta_1) - H_k(\bar{x}_{k|k-1} - \eta_1)\big) \tag{23}$$

Define $\epsilon := \frac{||\eta_2 - \eta_1||}{||\eta_2||}$ and ϵ_0 the desired parameter to stop the iteration, if $\epsilon > \epsilon_0$, repeat step 1 and step 2. After each iteration, $\eta_1 := \eta_2$.

3. New time update

After the iteration, the time update is obtained as follows:

$$\bar{x}_{k|k} = \eta_2 \tag{24}$$

$$P^{\bar{x}}_{k|k} = (I - K^{\bar{x}}_k H_k) P^{\bar{x}}_{k|k-1} (I - K^{\bar{x}}_k H_k)^T + K^{\bar{x}}_k R_k (K^{\bar{x}}_k)^T \tag{25}$$

The bias filter of the IOTSEKF, which is used to estimate the faults, is as follows:

$$\hat{f}^i_{k|k-1} = \hat{f}^i_{k-1|k-1} \tag{26}$$

$$\hat{f}^i_{k|k} = \hat{f}^i_{k|k-1} + K^{f^i}_k (y_k - H_k \bar{x}_{k|k-1} - S_k \hat{f}^i_{k|k-1}) \tag{27}$$

$$P^{f^i}_{k|k-1} = P^{f^i}_{k-1|k-1} + Q^{f^i}_{k-1} \tag{28}$$

$$K^{f^i}_k = P^{f^i}_{k|k-1} S^T_k (H_k P^{\bar{x}}_{k|k-1} H^T_k + R_k + S_k P^{f^i}_{k|k-1} S^T_k)^{-1} \tag{29}$$

$$P^{f^i}_{k|k} = (I - K^{f^i}_k S_k) P^{f^i}_{k|k-1} \tag{30}$$

and

$$\bar{u}_k = (\bar{U}_{k+1} - U_{k+1}) \hat{f}^i_{k|k} \tag{31}$$

$$\bar{Q}_k = Q_k - Q^{xf^i}_k \bar{U}^T_{k+1} - U_{k+1}(Q^{xf^i}_k - \bar{U}_{k+1} Q^{f^i}_k)^T \tag{32}$$

$$\bar{U}_k = \Phi_{k-1} V_{k-1} + \Gamma_{k-1} \tag{33}$$

$$S_k = H_k U_k \tag{34}$$

where U_k and V_k are the two-stage blending matrices which are given by

$$U_k = \bar{U}_k + (Q^{xf^i}_{k-1} - \bar{U}_k Q^{f^i}_{k-1})(P^{f^i}_{k|k-1})^{-1} \tag{35}$$

$$V_k = U_k - K^{\bar{x}}_k S_k \tag{36}$$

In the following two sections, the fault reconstructions of the liquid and solid OFC are shown.

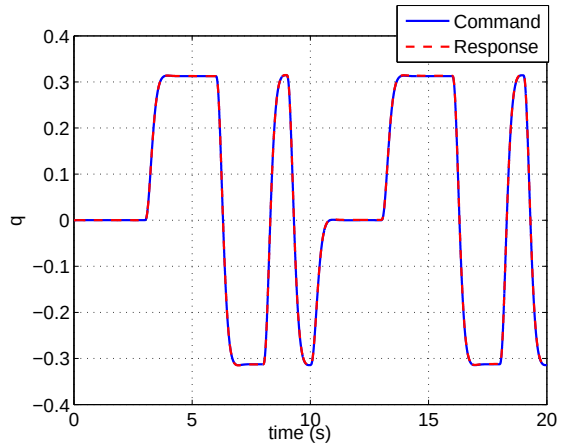

(a) Commanded q and its response

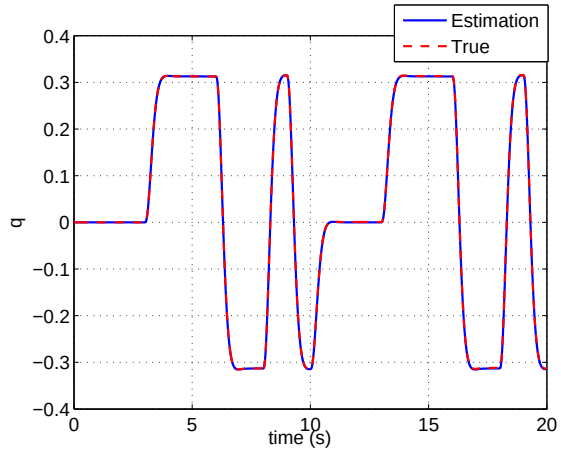

(b) True and estimated q

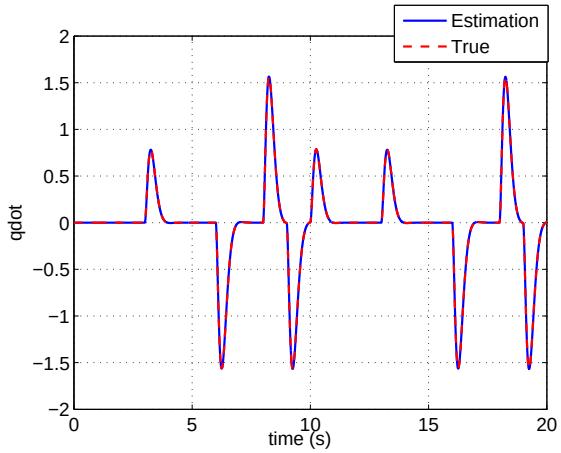

(c) True and estimated $\hat{q}$

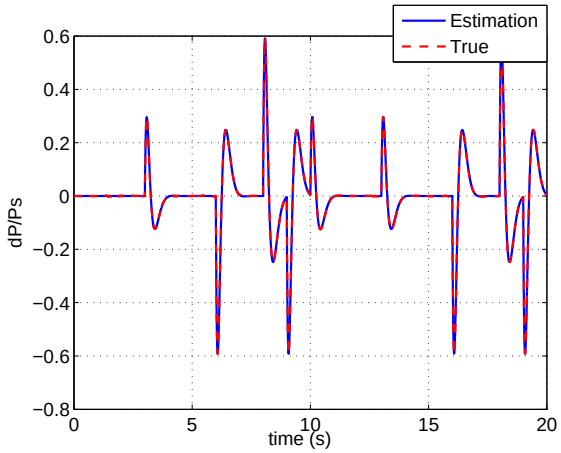

(d) True and estimated $\frac{\Delta P}{P_s}$

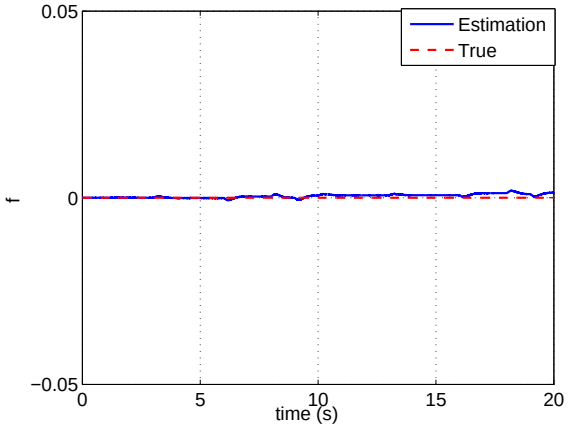

(e) Estimation of f^i

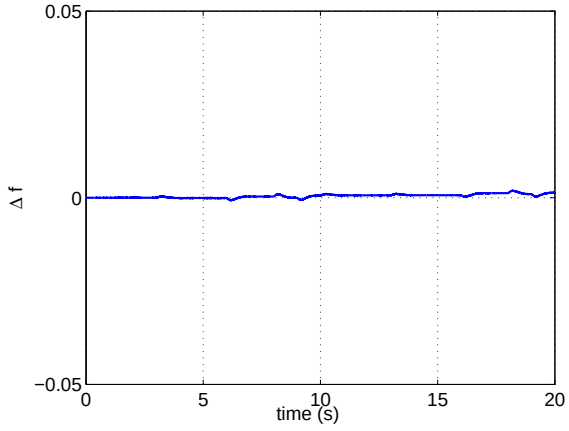

(f) Estimation error of f^i

Figure 2: Result of the liquid OFC reconstruction using the IOTSEKF

C. Fault-free scenario

The command given to the actuator is a 3-2-1-1 command. This section presents the results of the fault-free case where no faults are present. The results are shown in Fig. 2.

As can be seen from Fig. 2(a), the rod position of the actuator can follow the command very well. The estimation of the states are shown in Fig. 2(b), 2(c) and 2(d). As can be seen, all the states are estimated in an unbiased sense.

The fault estimation and estimation error are shown in Fig. 2(e) and 2(f) respectively. Since there are no faults, the estimation of the fault is close to zero.

D. Liquid OFC reconstruction

The fault reconstruction of the liquid OFC is shown in Fig. 3. Fig. 3(a) shows the reference command and the response of the actuator rod position. The rod position can follow the command well until the liquid fault is injected at $t = 12$ s.

The estimation of the states are shown in Fig. 3(b), 3(c) and 3(d). As can be seen, although in the presence of liquid OFC, the states are all estimated in an unbiased sense. It should be noted that these estimated states are used by the controller to design control laws.

The estimation of the fault is given by the blue solid line in Fig. 3(e). As can be seen, the fault signal is also estimated in an unbiased sense. The estimation error of the liquid OFC is shown in Fig. 3(f). After the injection of the liquid OFC, the estimation error increases slightly. In the case of a liquid OFC, the shape of the fault is only dependent on the fault itself. However, this is not the case when other fault scenarios occur, which will be seen from the following sections.

E. Solid OFC reconstruction

The solid OFC differs from the liquid OFC in that it substitutes the normal signal instead of being added to the normal signal. In this case, any effort to reduce the influence of the solid OFC will not have any impact.

The results of the solid OFC reconstruction is shown in Fig. 4. As can be seen from Fig. 4(a), after the injection of the solid OFC, the actuator rod position is no longer able to follow the command anymore and it only oscillates near the position when the fault is injected.

Even though the rod position can not be controlled to follow the command, the state estimation performance is still satisfactory, which is shown in Fig. 4(b), 4(c) and 4(d).

Finally, the fault estimation results are shown in Fig. 4(e) and 4(f) respectively. As can be seen from Fig. 4(e), the fault estimation follows the dynamics of the fault and the estimation error is small which is shown in Fig. 4(f). It should be noted that the shape of the solid OFC may change if the control signal input to the actuator is different. This is because the rod position is always an oscillatory signal, the fault changes with the change of the input signal.

V. Jamming and Runaway Fault Reconstruction

In the above section, the reconstructions of fault scenario 1 and 2 are introduced. In this section, the fault scenario 3, 4 and 5 will be dealt with.

First, some definitions of the jamming fault and runaway fault are given in section A. Then, in section B, the RTS-EKF is introduced which will be applied to deal with the fault reconstruction of the jamming and runaway faults. The results of the liquid jamming, solid jamming and runaway fault reconstruction are shown in sections C, D and E respectively.

A. Jamming and runaway

A jamming can include two types: liquid jamming and solid jamming. A liquid jamming is an additive bias occurs on the rod sensor while the control surface is still under control.[4] In this situation, the liquid jamming can be considered as a sensor fault, which is the output fault.

A solid jamming is the real case of a control surface jamming, which means that the control surface is stuck at its current position. The negative influence of the solid jamming is the resulting increased drag, which leads to more fuel consumption.

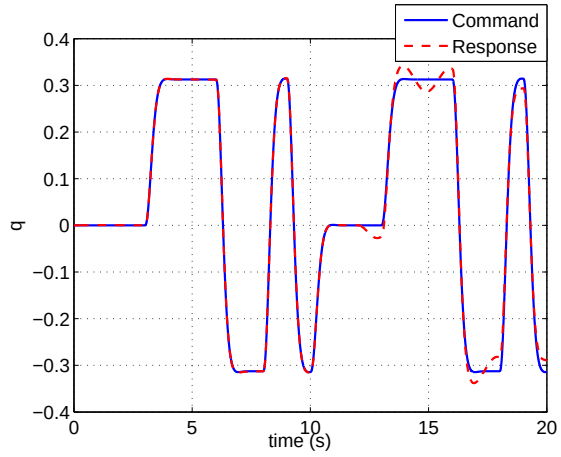

(a) Commanded q and its response

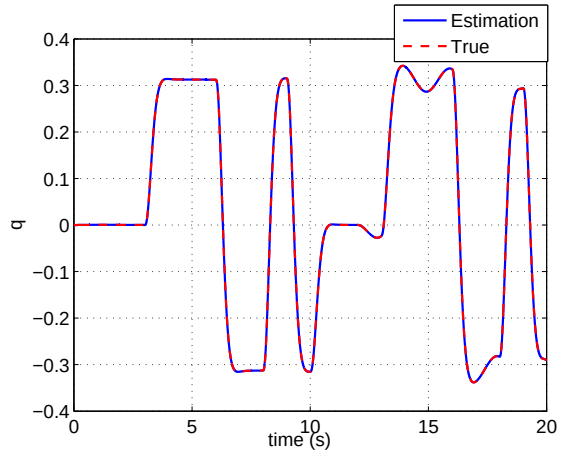

(b) True and estimated q

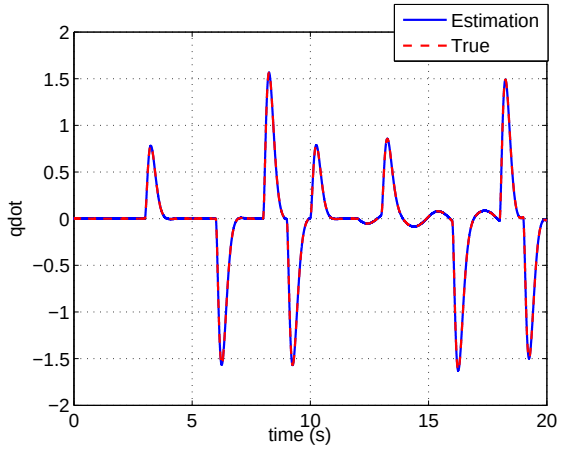

(c) True and estimated $\hat{q}$

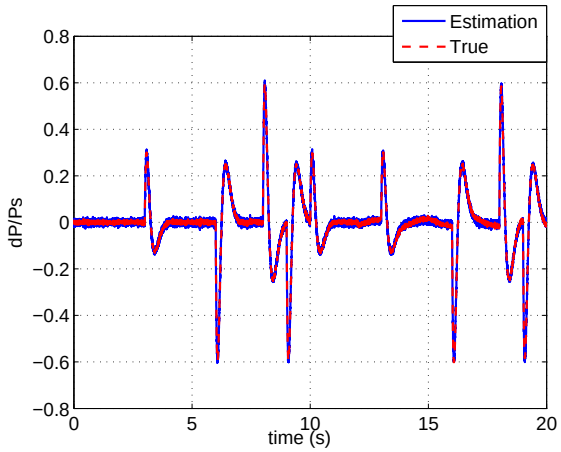

(d) True and estimated $\frac{\Delta P}{P_s}$

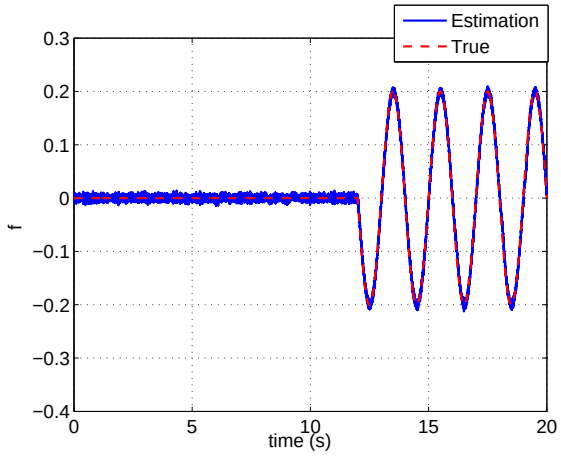

(e) Estimation of f^i

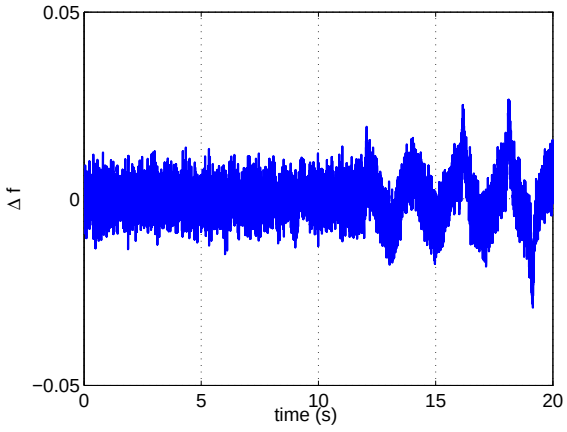

(f) Estimation error of f^i

Figure 3: Result of the liquid OFC reconstruction using the IOTSEKF

A runaway is an unwanted control surface deflection which, if undetected and stopped, persists until the moving surface stops.[4] Runaway is mainly caused by electronic component failure or mechanical breakage.

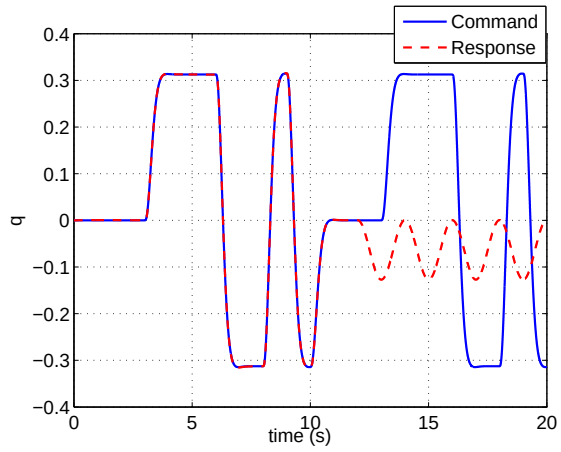

(a) Commanded q and its response

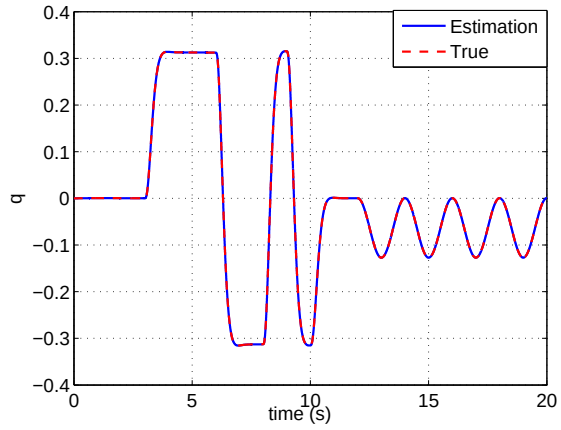

(b) True and estimated q

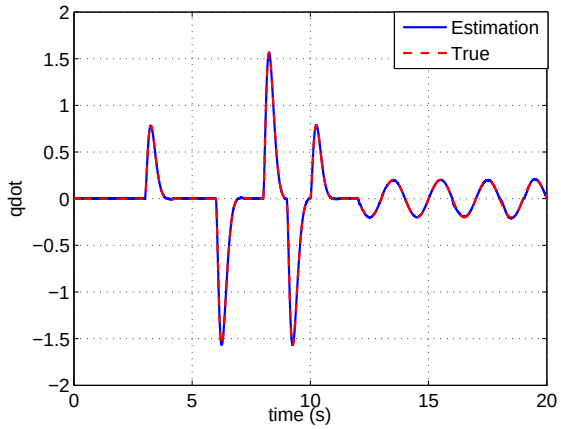

(c) True and estimated $\hat{q}$

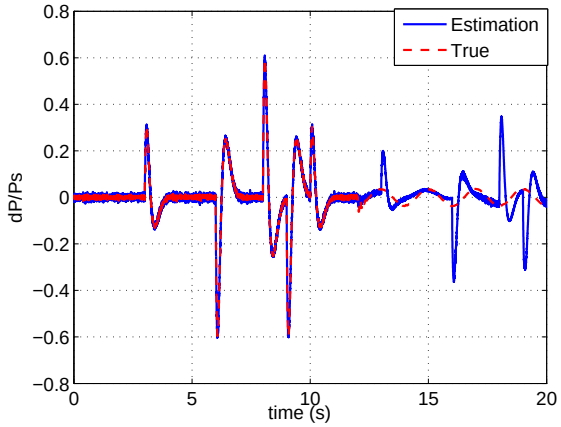

(d) True and estimated $\frac{\Delta P}{P_s}$

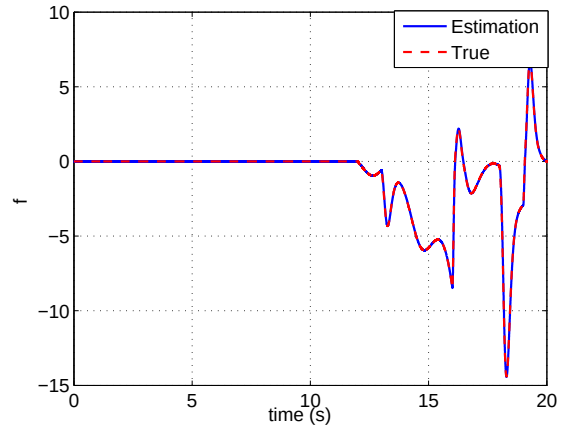

(e) Estimation of f^i

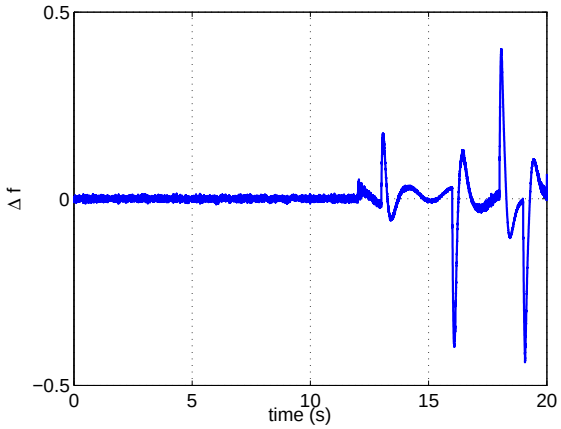

(f) Estimation error of f^i

Figure 4: Result of the solid OFC reconstruction using the IOTSEKF

It can result in an undesired maneuver or could require a local structural load augmentation in the aircraft. According the above definition, both the jamming and runaway fault can be considered as output fault

of the actuator. Therefore, they are all dealt with in this section.

An unbiased estimation of the state and the output faults can be achieved using a RTS-EKF[11] which is introduced in the following.

B. Robust Three-Step Extended Kalman Filter

This section designs a RTS-EKF[19,11] for the jamming and runaway fault reconstruction. Consider the actuator model described by Eqs. (1) and (2). For this system, the existence condition of a RTS-EKF is:[19,11]

$$m \geq p, \qquad \text{rank } F_k = p \tag{37}$$

where $F_k = I$ is the fault distribution matrix. In this study, $m = 1$ and $p = 1$. Therefore, a RTS-EKF can be designed. The state and the fault can be estimated by designing the following three-step filter:

Step1 Time update

$$\hat{x}_{k|k-1} = \hat{x}_{k-1|k-1} + \int_{k-1}^{k} f(x(t), u(t), f^i(t))dt \tag{38}$$

$$P_{k|k-1} = \Phi_{k-1} P_{k-1|k-1} \Phi_{k-1}^T + Q_k^d \tag{39}$$

where $\hat{x}_{k-1|k-1}$ and $P_{k-1|k-1}$ are the state estimation and covariance of the state estimation error at step $k-1$, respectively. Q_k^d is computed by:

$$Q_k^d = \int_{t_{k-1}}^{t_k} \Phi_{k-1} G(\hat{x}_{k-1|k-1}) Q_{k-1} G^T(\hat{x}_{k-1|k-1}) \Phi_{k-1}^T d\tau.$$

Step2 Estimation of the faults

$$\tilde{R}_k = H_k P_{k|k-1} H_k^T + R_k \tag{40}$$

$$\gamma_k' = y_k - H_k \hat{x}_{k|k-1} \tag{41}$$

$$\hat{f}_k^o = N_k \gamma_k' \tag{42}$$

$$P_k^f = (F_k^T \tilde{R}_k^{-1} F_k)^{-1} \tag{43}$$

with

$$H_k = \frac{\partial h(x(t), f^o(t))}{\partial x}|_{x=\hat{x}_{k|k-1}}. \tag{44}$$

$\hat{f}_k^o$ is the estimation of the output fault f_k^o and P_k^f is the error covariance matrix of the fault estimation.

Step3 Measurement update

$$K_k = P_{k|k-1} H_k^T \tilde{R}_k^{-1} \tag{45}$$

$$\hat{x}_{k|k} = \hat{x}_{k|k-1} + K_k(y_k - H_k \hat{x}_{k|k-1} - F_k \hat{f}_k^o) \tag{46}$$

$$P_{k|k} = P_{k|k-1} - K_k(\tilde{R}_k - F_k P_k^f F_k) K_k^T \tag{47}$$

The optimal estimation in the unbiased minimum variance sense of the fault can be obtained by[19]

$$N_k = (F_k^T \tilde{R}_k^{-1} F_k)^{-1} F_k^T \tilde{R}_k^{-1} \tag{48}$$

It is proved that the RTS-EKF can achieve an unbiased state and fault estimation simultaneously.[19] The fault reconstruction of the jamming and runaway using the RTS-EKF is shown in the following.

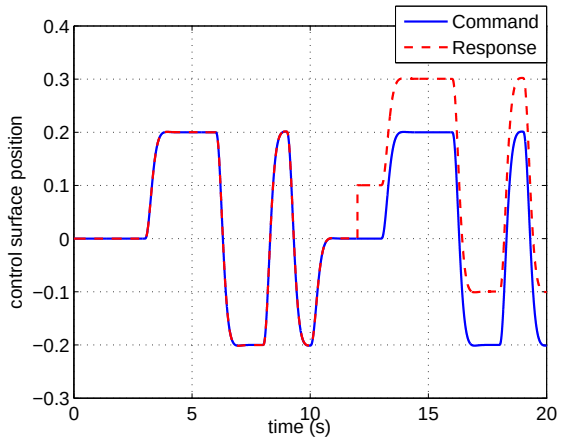

(a) Commanded and true position of the control surface

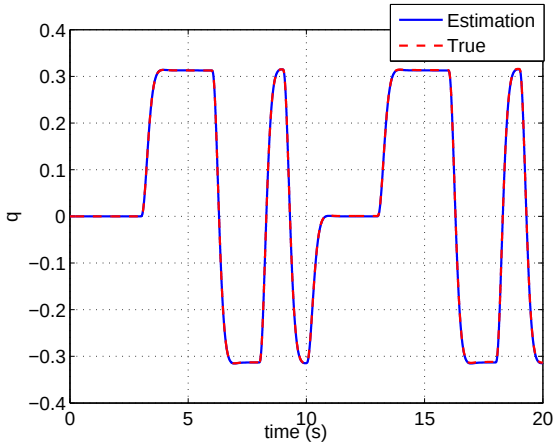

(b) True and estimated q

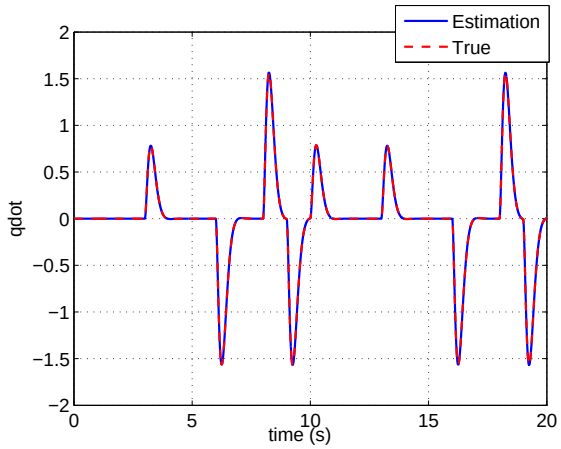

(c) True and estimated $\hat{q}$

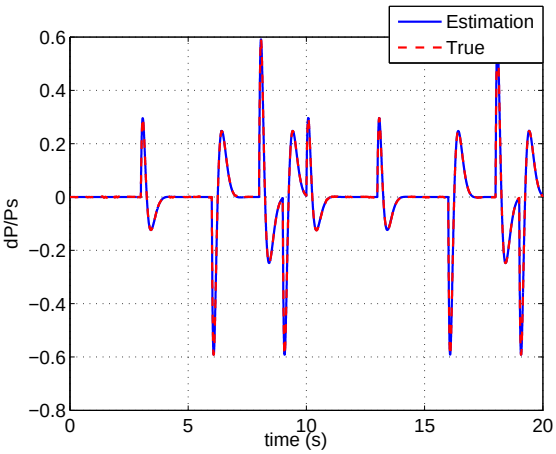

(d) True and estimated $\frac{\Delta P}{P_s}$

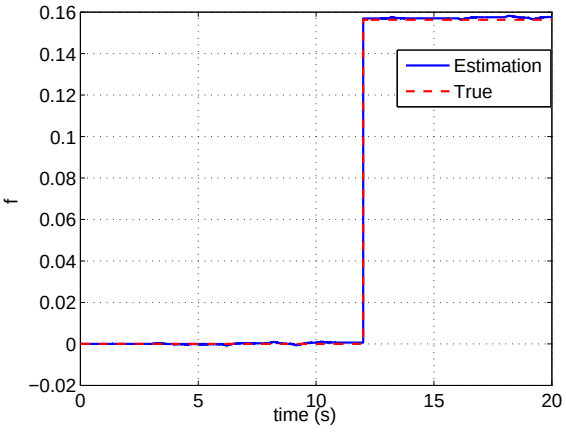

(e) Estimation of f^i

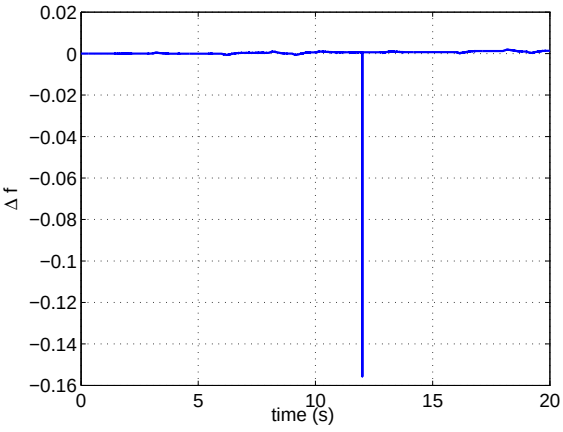

(f) Estimation error of f^i

Figure 5: Result of the liquid jamming reconstruction using the RTS-EKF

C. Liquid jamming fault reconstruction

In this section, the liquid jamming fault reconstruction is considered. The fault is injected at $t = 12$ s. The results of the liquid jamming fault reconstruction is shown in Fig. 5.

As can be seen from Fig. 5(a), the control surface deflection deviates from the command after the liquid jamming fault is injected. This also shows the influence of the rod sensor. If the sensor measurement is not correct, the control surface will not follow the command.

The estimates of q, $\dot{q}$ and $\frac{\Delta P}{P_s}$ are shown in Fig. 5(b), 5(c) and 5(d) respectively. As can be seen, the RTS-EKF is able to estimate the states when the sensor is in error. This is due to the property of the RTS-EKF which can decouple the state and disturbance.

The fault reconstruction results using the RTS-EKF are shown in Fig. 5(e) and 5(f) respectively. It is seen that the bias sensor fault is estimated in an unbiased sense. In this case, the shape of the fault does not depend on the position of the control surface command.

D. Solid jamming fault reconstruction

The solid jamming fault reconstruction results are shown in Fig. 6. The control surface position is shown in Fig. 6(a). Since the jamming is injected at $t = 12$ s, when the position of the control surface is close to zero, the control surface position remains at the null-position.[4] In this case, no effort can control the surface to follow the command.

Even though the control surface is stuck at the null-position, the states of the actuator are still estimated in an unbiased sense, which can be seen from Fig. 6(b), 6(c) and 6(d). These correct estimation of the states are used by the controller.

Finally, the estimation of the fault is shown in Fig. 6(e). The difference from the true fault is shown in Fig. 6(f). It is seen that the estimated fault matches closely with the true fault. It should be noted that in this case, the shape of the fault depends on the commanded position and the position where the control surface is stuck.

E. Runaway fault reconstruction

The runaway fault is also an output fault of the actuator. The results of the runaway fault reconstruction using the RTS-EKF is shown in Fig. 7.

The position of the control surface is shown in Fig. 7(a). As can be seen, after the occurrence of the fault, the control surface deviates from the commanded position and is stuck at the limit. In this case, there is also no effort can control the surface to follow the command.

The estimation of the states is unbiased as expected. The estimates of q, $\dot{q}$ and $\frac{\Delta P}{P_s}$ are shown in Fig. 7(b), 7(c) and 7(d) respectively.

Again the fault reconstruction is shown in Fig. 7(e). It can be seen the fault reconstruction is unbiased whose error is shown in Fig. 7(f). The estimation error is zero-mean and is satisfactory. It should also be noted that in this case, the shape of the fault is also dependent on the runaway speed and the control surface command. Different runaway speeds will result into different fault shapes.

VI. Conclusions

This paper deals with the actuator fault reconstruction problem. First, the general actuator model is given which includes the faults. A Nonlinear Dynamic Inversion (NDI) controller is designed for the actuator. Then, the complete actuator fault reconstruction system is given. It is composed of a reference model, a controller and a fault estimation.

The considered actuator fault types include: liquid and solid Oscillatory Failure Case (OFC), liquid and solid jamming and runaway fault. These faults are modeled as input or output faults of the actuator. Therefore, two different fault reconstruction systems are designed. One is based on the Iterated Optimal Two-Stage Extended Kalman Filter (IOTSEKF) which can estimate the state and input fault in an unbiased sense. The liquid and solid OFC can be reconstructed using this IOTSEKF. The other fault reconstruction system is based on the Robust Three-Step Extended Kalman Filter (RTS-EKF) which can estimate the state and reconstruct the output faults in an unbiased sense. This fault reconstruction system can cope with the reconstruction of the liquid and solid jamming and the runaway fault.

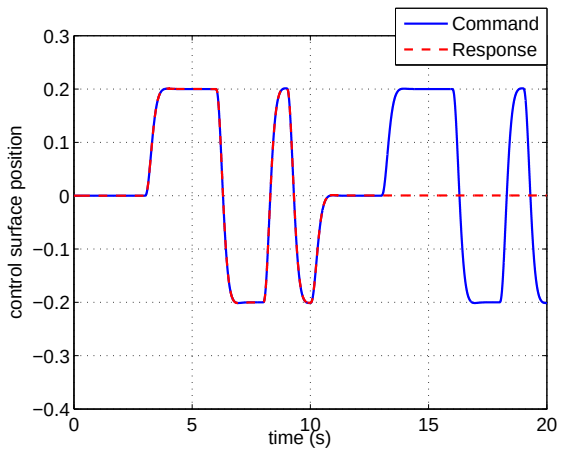

(a) Commanded and true position of the control surface

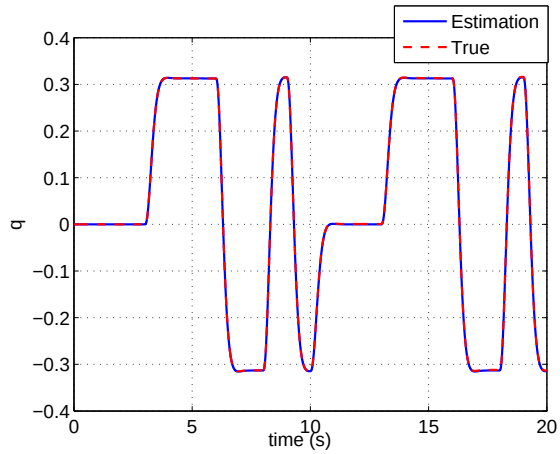

(b) True and estimated q

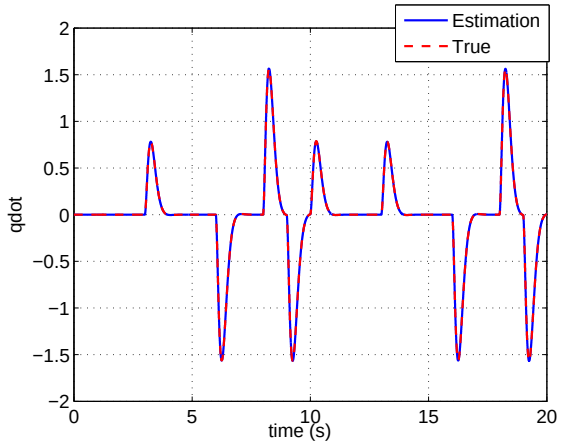

(c) True and estimated $\hat{q}$

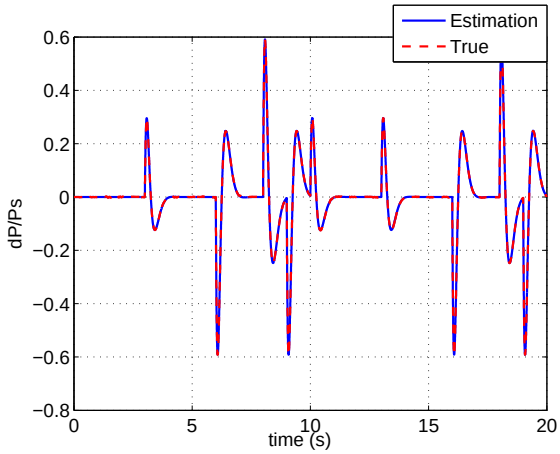

(d) True and estimated $\frac{\Delta P}{P_s}$

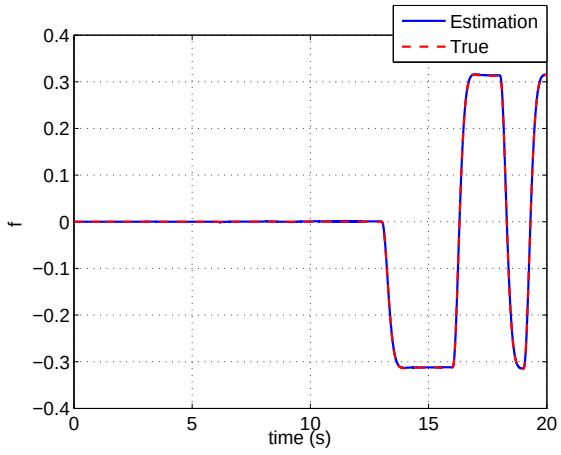

(e) Estimation of f^i

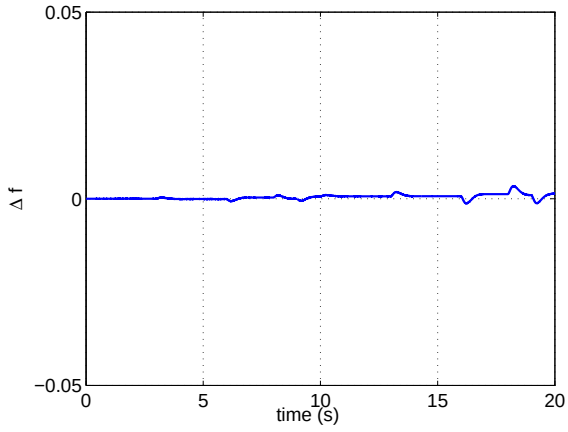

(f) Estimation error of f^i

Figure 6: Result of the solid jamming reconstruction using the RTS-EKF

The performance of the proposed actuator fault reconstruction systems is validated using five different fault scenarios. The simulation results demonstrate the effectiveness of the proposed systems. This also

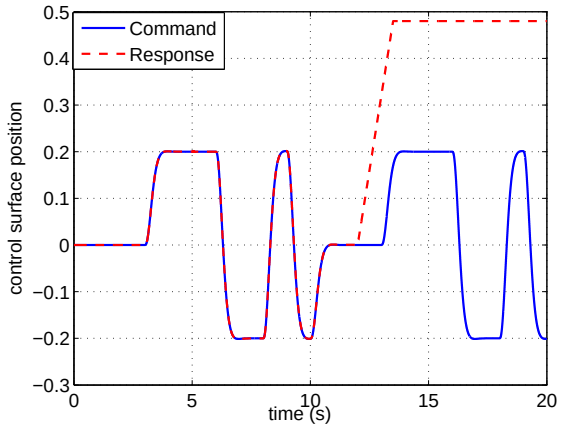

(a) Commanded and true position of the control surface

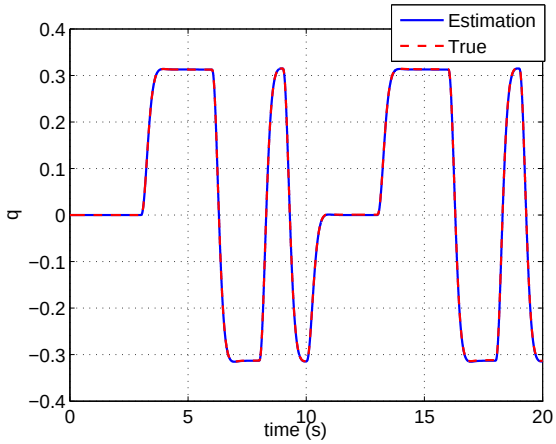

(b) True and estimated q

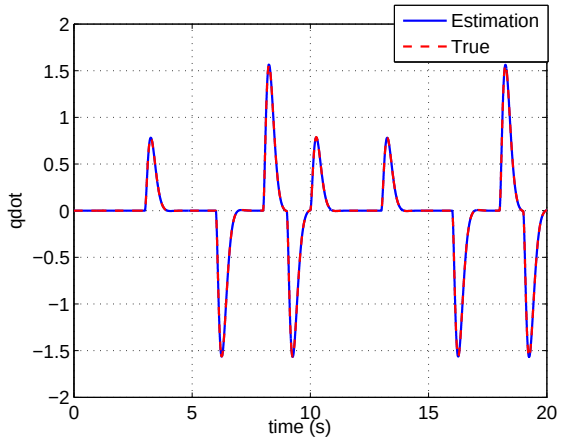

(c) True and estimated $\hat{q}$

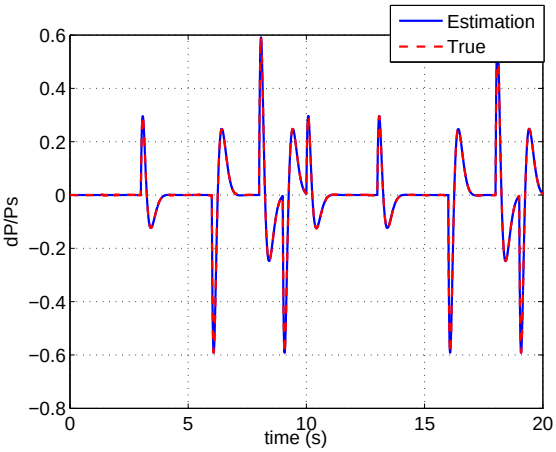

(d) True and estimated $\frac{\Delta P}{P_s}$

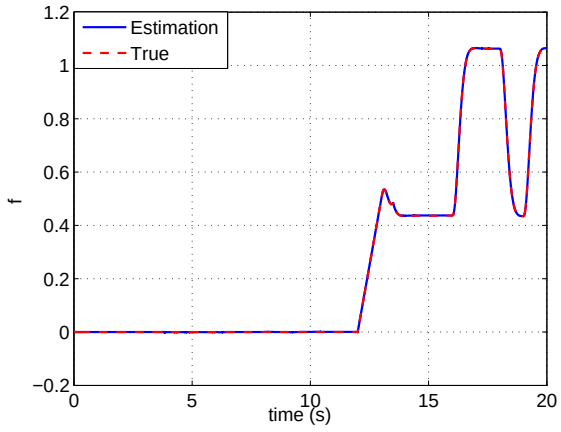

(e) Estimation of f^i

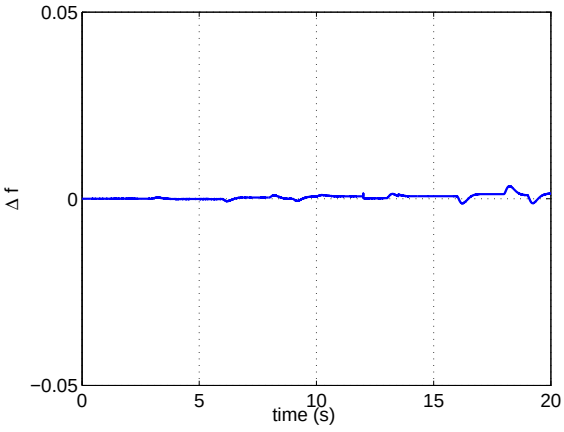

(f) Estimation error of f^i

Figure 7: Result of the runaway reconstruction using the RTS-EKF

indicates that the proposed systems can be incorporated into the actuator system to perform the fault detection and reconstruction.

References

[1]Chen, J. and Patton, R. J., *Robust model-based fault diagnosis for dynamic systems*, Kluwer Academic Publishers, Norwell, MA, USA, 1999.

[2]Isermann, R., "Model-based fault-detection and diagnosis- status and applications," *Annual Reviews in Control*, Vol. 29, No. 1, Jan. 2005, pp. 71–85.

[3]Venkatasubramanian, V., Rengaswamy, R., and Yin, K., "A review of process fault detection and diagnosis Part I : Quantitative model-based methods," *Computers and Chemical Engineering*, Vol. 27, 2003, pp. 293–311.

[4]Goupil, P. and Marcos, A., "The European ADDSAFE project: Industrial and academic efforts towards advanced fault diagnosis," *Control Engineering Practice*, Vol. 31, No. July 2009, 2014, pp. 109–125.

[5]Patton, R. J., "Fault-tolerant Control Systems: The 1997 Situation," *Proc. of IFAC Symp. on Fault Detection, Supervision and Safety for Technical Processes*, 1997, pp. 1033–1054.

[6]Marzat, J., Piet-Lahanier, H., Damongeot, F., and Walter, E., "Model-based fault diagnosis for aerospace systems: a survey," *Proceedings of the Institution of Mechanical Engineers, Part G: Journal of Aerospace Engineering*, Vol. 226, No. 10, Jan. 2012, pp. 1329–1360.

[7]Van Eykeren, L. and Chu, Q., "Fault Detection and Isolation for Inertial Reference Units," *AIAA Guidance, Navigation and Control Conference*, Boston, MA, 2013, pp. 1–10.

[8]Lu, P., Van Eykeren, L., van Kampen, E., de Visser, C. C., and Chu, Q., "Double-model adaptive fault detection and diagnosis applied to real flight data," *Control Engineering Practice*, Vol. 36, March 2015, pp. 39–57.

[9]Van Eykeren, L. and Chu, Q., "Sensor fault detection and isolation for aircraft control systems by kinematic relations," *Control Engineering Practice*, Vol. 31, 2014, pp. 200–210.

[10]Lu, P., Van Eykeren, L., van Kampen, E., and Chu, Q., "Selective-Reinitialisation Multiple Model Adaptive Estimation for Fault Detection and Diagnosis," *Journal of Guidance, Control, and Dynamics*, Vol. 38, No. 8, 2015, pp. 1409–1425.

[11]Lu, P., Van Eykeren, L., van Kampen, E., de Visser, C. C., and Chu, Q., "Adaptive Three-Step Kalman Filter for Air Data Sensor Fault Detection and Diagnosis," *Journal of Guidance, Control, and Dynamics*, 2015, pp. 1–15 (available online).

[12]Lu, P. and van Kampen, E., "Aircraft Inertial Measurement Unit Fault Identification with Application to Real Flight Data," *AIAA Guidance, Navigation and Control Conference*, No. AIAA 2015-0859, Kissimmee, Florida, 2015, pp. 1–17.

[13]Goupil, P., "Oscillatory failure case detection in the A380 electrical flight control system by analytical redundancy," *Control Engineering Practice*, Vol. 18, No. 9, Sept. 2010, pp. 1110–1119.

[14]Alwi, H. and Edwards, C., "Second order sliding mode observers for the ADDSAFE actuator benchmark problem," *Control Engineering Practice*, Vol. 31, Oct. 2014, pp. 74–91.

[15]Varga, A. and Ossmann, D., "LPV model-based robust diagnosis of flight actuator faults," *Control Engineering Practice*, Vol. 31, 2013, pp. 135–147.

[16]Schothorst, G. V., *Modelling of Long-Stroke Hydraulic Servo-Systems*, Ph.D. thesis, Delft University of Technology, 1997.

[17]Van Eykeren, L. and Chu, Q. P., "Nonlinear Model-Based Fault Detection for a Hydraulic Actuator," *AIAA Guidance, Navigation, and Control Conference*, No. August, Portland, Oregon, 2011, pp. 1–8.

[18]Hsieh, C.-S. and Chen, F.-G., "Optimal Solution of the Two-Stage Kalman Estimator," *IEEE Transactions on Automatic Control*, Vol. 44, No. 1, 1999, pp. 194–199.

[19]Gillijns, S. and De Moor, B., "Unbiased minimum-variance input and state estimation for linear discrete-time systems with direct feedthrough," *Automatica*, Vol. 43, No. 5, May 2007, pp. 111–116.